Finite Blade Functions and Blade Element Optimization for Diffuser-augmented Wind Turbines

Vaz, Jerson R.P.; Okulov, Valery L.; Wood, David H.

Published in:
Renewable Energy

Link to article, DOI:
10.1016/j.renene.2020.11.059

Publication date:
2021

Document Version
Peer reviewed version

Journal Pre-proof

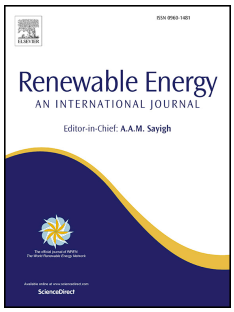

Finite Blade Functions and Blade Element Optimization for Diffuser-augmented Wind Turbines

Jerson R.P. Vaz, Valery L. Okulov, David H. Wood

PII: S0960-1481(20)31802-4

DOI: https://doi.org/10.1016/j.renene.2020.11.059

Reference: RENE 14500

To appear in: *Renewable Energy*

Received Date: 4 April 2020

Revised Date: 11 August 2020

Accepted Date: 12 November 2020

Please cite this article as: Vaz JRP, Okulov VL, Wood DH, Finite Blade Functions and Blade Element Optimization for Diffuser-augmented Wind Turbines, *Renewable Energy*, https://doi.org/10.1016/j.renene.2020.11.059.

Credit Author Statement

Jerson R. P. Vaz
Methodology, Investigation, Writing – Original Draft, Visualization

Valery L. Okulov
Supervision, Project Administration, Funding Acquisition, Writing – Review & Editing

David H. Wood
Conceptualization, Methodology, Writing – Original Draft, Writing – Review & Editing, Visualization

Finite Blade Functions and Blade Element Optimization for Diffuser-augmented Wind Turbines

Jerson R. P. Vaz[a,*], Valery L. Okulov[b,c], David H. Wood[d]

[a] *Faculty of Mechanical Engineering, Institute of Technology, Federal University of Pará - Av. Augusto Correa, N 1 - Belém, PA, 66075-900, Brazil*
[b] *Wind Energy Department, DTU, Nils Koppels Alle 403, 2800 Lyngby, Denmark*
[c] *Novosibirsk State University, Pirogova Street. 2, 630090, Novosibirsk-90, Russia*
[d] *Department of Mechanical and Manufacturing Engineering, Schulich School of Engineering, University of Calgary, Calgary T2N 1N4, Alberta, Canada.*

*Corresponding author
Email address: jerson@ufpa.br (Jerson R. P. Vaz)

Finite Blade Functions and Blade Element Optimization for Diffuser-augmented Wind Turbines

Jerson R. P. Vaz[a,*], Valery L. Okulov[b,c], David H. Wood[d,c]

[a] *Faculty of Mechanical Engineering, Institute of Technology, Federal University of Pará - Av. Augusto Correa, N 1 - Belém, PA, 66075-900, Brazil*
[b] *Wind Energy Department, DTU, Nils Koppels Alle 403, 2800 Lyngby, Denmark*
[c] *Novosibirsk State University, Pirogova Street. 2, 630090, Novosibirsk-90, Russia*
[d] *Department of Mechanical and Manufacturing Engineering, Schulich School of Engineering, University of Calgary, Calgary T2N 1N4, Alberta, Canada.*

Abstract

Placing a diffuser around a wind turbine can increase its power output, but not all mechanisms by which the diffuser alters the aerodynamics have been investigated thoroughly. Here, we concentrate on one such mechanism: the effect of the finite number of blades. In nearly all blade element analyses of wind turbines, finite blade effects are approximated by Prandtl's "tip loss factor" which goes to zero at the blade tip. We argue that this limiting behaviour cannot be correct for the axial velocity in the presence of a diffuser. We provide alternative "finite blade functions" which preserve the finite limit on the axial velocity, but do not alter the conventional limit of zero for the circumferential velocity. In maximizing the power output of a diffuser-augmented wind turbine, the change in the finite blade function for the axial velocity has a large impact on the power-producing region near the tip: it increases both the chord and the power output of an optimized blade. Further, the change appears to make diffuser-augmented turbine power output less sensitive to tip speed ratio than for a bare turbine.

Keywords: Tip loss, DAWT, Diffuser, Blade Element Theory.

*Corresponding author
Email address: jerson@ufpa.br (Jerson R. P. Vaz)

1. Introduction

It is well-known that diffuser augmentation of a wind turbine can increase the power output, e.g Jamieson [1]. This increase is proportional to the flow rate of air induced through the rotor by the diffuser, e.g. Hansen et al. [2], showing the importance of the diffuser design, a subject that has been studied extensively, e.g. Hjort & Larsen [3]. No large diffuser-augmented wind turbines (DAWTs) have been commercially successful, but there is a strong potential for small DAWTs in urban areas, where the wind conditions and the specific needs for safety favour the concept, e.g. Anup et al. [4] and Dilimulati et al. [5]. Diffuser-augmented hydrokinetic turbines (DAHKTs) also have promise for rivers and tidal flows, e.g. Silva et al. [6]. Even for these applications, however, there is some doubt as to whether the increase in total mass, size, and cost over a bare turbine is beneficial, e.g Lubitz & Shomer [7]. It follows that DAWTs need to be aggressively optimized.

Adding a diffuser is simple in concept, but often complex to analyze, even when using basic blade element momentum theory (BEMT), the main workhorse for the study of bare turbines, e.g. Hansen [8]. The diffuser can be modeled using computational fluid dynamics (CFD), e.g, [3] and Kesby et al. [9], and, clearly, its performance is influenced by interaction with the blades. If CFD is not used, it is often assumed that the diffuser is perfectly efficient, although methods to include finite efficiency have been available for a long time, e.g. Fletcher [10], who ignored diffuser thrust, and Vaz & Wood [11] who included it.

This paper concentrates on an aspect of BEMT for DAWTs that has received little attention: the accounting for the finite number of blades, N. This is routinely done in BEMT for any turbine by using Prandtl's "tip loss factor", F_P, in the form developed by Glauert [12], see also Sørensen [13]. Finite N causes the induced velocities at the blades to differ from the streamtube averages. Following the paragraph before Eq. (5.3) in Glauert [12], the axial, F_u, and circumferential, F_w, "finite blade functions" can be written in terms of the induced axial and circumferential velocities, a, and a' respectively, as

$$F_u = a/a_b \quad \text{and} \quad F_w = a'/a_b^{'}, \tag{1}$$

where the subscript "b" denotes a value at the blade and a symbol without "b" denotes a streamtube average. The calculation of the induced velocities is described in Section 3. The standard approximation is $F_u = F_w = F_P$, where

$F_P \leq 1$. For bare turbines, a difference between F_u and F_w was considered, but not used, by Shen et al. [14], while Wimhurst & Willden [15] determined F_u and F_w using a three-dimensional computational simulation. As $N \to \infty$, $F_P, F_u, F_w \to 1$ because there is no difference between a and a_b, or between a' and a'_b, for an actuator disk. Further, F_P goes to zero at the blade tip and has a strong influence on the torque and thrust acting on the blade elements in the outer part of a blade.

We believe that "tip loss factor" is not a good name for F_u and F_w, and will continue to use the more general "finite blade functions" which covers the following situations. If the blades have "pre-bend" or are "coned", that is they do not lie entirely in the radial plane, then the velocity at each element is influenced by the bound circulation of every other element, e.g. Wood [16]. If the blades are unequally loaded, due to wind shear or yaw, there are "cascade" effects from the other blade elements at the same radius, Wood [17]. These cases, which cannot be modeled by F_P, are not considered here because F_P has an even more important deficiency for DAWTs: it is zero at the tip for both the axial and circumferential flow. A diffuser, however, *induces* an axial velocity through the rotor that may vary radially, but not circumferentially. This situation does not correspond to the idealized vortex sheet model that was probably used by Prandtl to derive his tip loss formula, see Glauert [12] and Sørensen [13]. Since all induced velocities must be included in Eq. (1), F_u cannot be zero at the blade tip in a DAWT, but F_w can be zero. The tip region of a DAWT has some similarities to the tip regions of a gas turbine which have much more complex flow, but the presence of the end wall prevents complete unloading at the tip. Figure 11 of Passman et al. [18], for example, shows the blade loading for a simplified blade model at 95% span is not significantly reduced from the value at midspan. The secondary vortex formation that is associated with tip effects must occur for DAWTs of sufficiently small tip clearance but we are unaware of any detailed study of them. Ironically, these tip effects are not captured by the "tip loss factor". The present analysis using a simple model for F_u and F_w can be viewed as a small step in the direction of improved tip modeling.

We consider a DAWT with the simplest configuration of straight, unconed, equally-loaded blades, because then only the trailing vorticity can change the blade element velocities from the streamtube averages. We develop the analysis of Wood & Okulov [16] and [19] for bare turbines. They used Okulov's [20] approximations to the Kawada-Hardin (KH) equations for the velocity field induced by a semi-infinite helical vortex of constant ra-

dius and pitch, see Fukumoto et al. [21]. The equations are applied to the vortices trailing from the junctions of all blade elements, as well as the hub and tip, to compute the velocities at the centre of each element. Because of the restriction to vortices of constant radius and pitch, the KH equations are undoubtedly simplistic. In principle, the resulting finite blade functions are less accurate that could be obtained numerically, e.g. [15]. On the other hand the equations are analytic and are straightforward to combine with a BEMT computation.

The KH equations and Okulov's approximations have the important characteristic that [16] and [19] called "Kawada cancellation"; the velocity variations in the circumferential direction due to N equally-spaced helical vortices of the same strength, Γ, tend to zero as $N \to \infty$ so that F_u and F_w tend to unity in the same limit. The results in [16] and [19] show that F_u and F_w increasingly differ from F_P as tip speed ratio, λ is reduced. Although it is not the primary reason to study finite blade functions for DAWTs, we note that their typical λ is lower than for bare turbines.

In this paper, we describe for the first time the determination of F_u and F_w for a DAWT, and their use in a blade element analysis to determine thrust and power. The BEMT method of Vaz & Wood [11], which includes the diffuser efficiency and thrust, is modified by replacing F_P by F_u or F_w where appropriate. We also adjust their expression for the axial velocity at the rotor. The next Section summarizes vortex theory for DAWTs. The following Section describes the integration of F_u and F_w into a BEMT optimization. Section 4 details the calculation of the finite blade functions, and then Section 5 describes the simulated DAWT. Section 6 gives the results. The last Section, 7, contains the conclusions.

2. Vortex Theory for DAWTs

Fig. 1 depicts a DAWT with $N = 2$; this number is used in the figure only for convenience as the following analysis holds for any N. A vortex sheet continuously sheds from each blade with an induced axial velocity of w. V_0 is the freestream velocity, and Ω is the angular speed of the rotor. In the absence of the rotor, the diffuser induces an extra flow whose axial velocity at the rotor position is V_d, which may be a function of radius, r, but not of the circumferential co-ordinate. When the turbine is operating, the axial velocity at the rotor is V_1. Therefore, the diffuser maximizes F_u at the tip relative to F_p. V_1, however, will differ from its value when there is no rotor,

$V_0 + V_d$, in a manner similar to the difference between V_0 and the velocity of the rotor of a bare turbine.

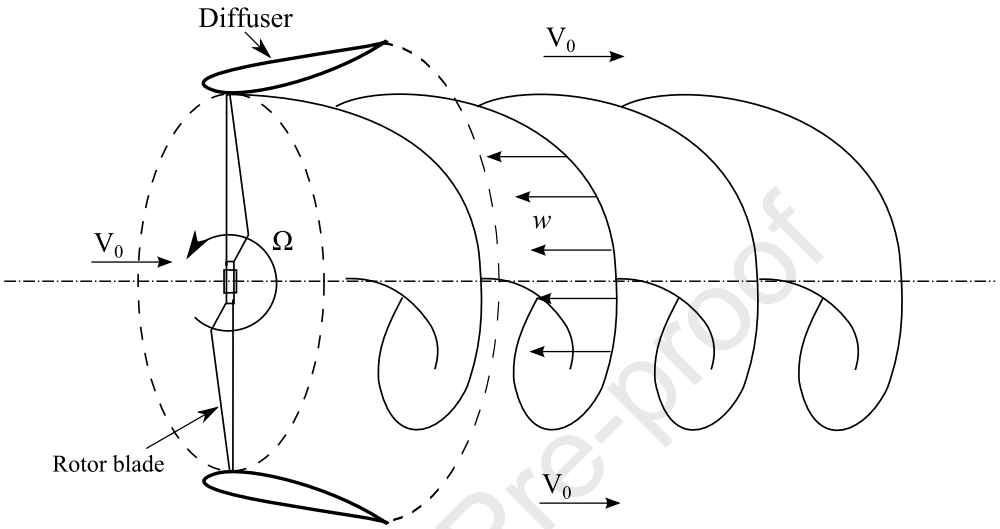

Figure 1: Simplified illustration of the helical surface of an ideal wake of a diffuser-augmented wind turbine, adapted from Okulov & Sørensen [22].

The following exposition of geometric aspects of vortex theory for a DAWT is a straightforward development of that in Okulov & Sørensen [22] for a bare turbine. The major addition is V_d, which may be calculated simply by applying the momentum equation to the control volume shown in Fig. 2 for an empty diffuser. Hence, the energy balance downstream of the diffuser exit, denoting the losses as ΔH, gives:

$$1 = c_{p3} + \beta^2 \left(\frac{V_1}{V_0} \right)^2 + \frac{\Delta H}{\frac{1}{2}\rho V_0^2}, \tag{2}$$

where β is the diffuser area ratio, and the pressure coefficient, c_{p3}, at the diffuser outlet is

$$c_{p3} = \frac{p_3 - p_0}{\frac{1}{2}\rho V_0^2}, \tag{3}$$

in which p_0 is the static pressure in the external flow, [11]. Introducing the

diffuser efficiency, η_d, the losses are computed through

$$\Delta H = \frac{1}{2}\rho V_0^2 \left(\frac{V_1}{V_0}\right)^2 (1-\eta_d)\left(1-\beta^2\right), \tag{4}$$

so that $\Delta H = 0$ if $\eta_d = 1$. The total velocity at the rotor plane of the empty diffuser is $V_0 + V_d$, yielding in normalized form:

$$v_d = \frac{V_d}{V_0} = \sqrt{\frac{1-c_{p3}}{\beta^2 + (1-\eta_d)\left(1-\beta^2\right)}} - 1. \tag{5}$$

Thus V_d is independent of r but dependent on the pressure coefficient at the diffuser exit, area ratio, and the diffuser efficiency.

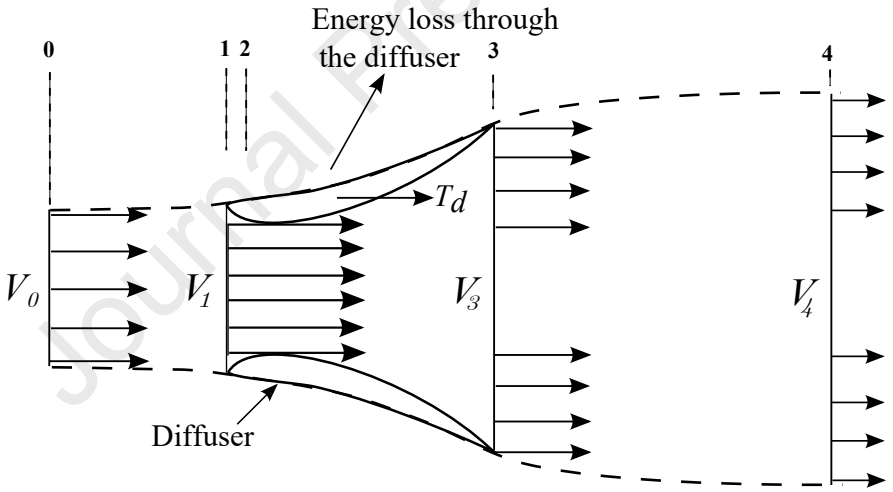

Figure 2: Control volume of an empty diffuser.

According to the velocity diagram in Fig. 3, the total axial velocity of the vortex sheet is $V_0 - w + V_d = V_1 - w$. V_d influences the pitch, p, of the helicoidal wake because the dimensionless form of $p(r)$ is

$$\frac{p}{r} = \tan\phi = \frac{V_0 - w + V_d}{\Omega r}, \tag{6}$$

where ϕ is the angle between the vortex sheet and the rotor plane defined in

Fig. 3. For completeness, we note that p can also be written as

$$p = \frac{1}{\tilde{\lambda}} \left(1 - \tilde{w}\right), \tag{7}$$

where the "modified tip speed ratio" $\tilde{\lambda} = \Omega R / V_1$ and $\tilde{w} = w/V_1$. This equation is not used in the present analysis.

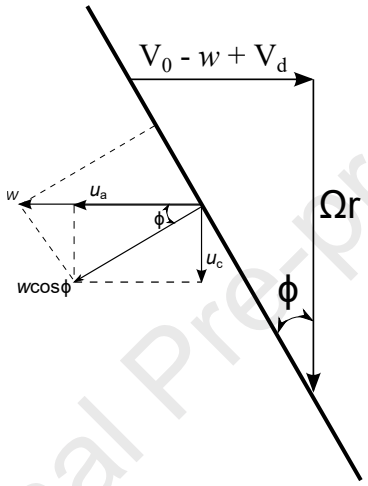

Figure 3: Velocity diagram for the vortex sheet of a DAWT, adapted from Okulov & Sørensen [22].

The axial and circumferential velocity components induced by the sheet are the same as for a bare turbine. As given by Okulov & Sørensen [22], the axial velocity, u_a, induced by the helix is

$$u_a = w \cos^2 \phi = \frac{w r^2}{p^2 + r^2}. \tag{8}$$

Similarly, the equation for the circumferential induced velocity, u_c, is

$$u_c = w \sin \phi \cos \phi = \frac{w r p}{p^2 + r^2}. \tag{9}$$

Extending Eq. (24) of Okulov & Sørensen [22], ϕ is also given by

$$\tan \phi = \frac{V_0 - u_a + V_d}{\Omega r + u_c} = \frac{V_1 - u_a}{\Omega r + u_c}. \tag{10}$$

The bound circulation of each element, Γ, needed later to determine u_a

and u_c, comes from the torque acting on the blade element:

$$\Gamma = \frac{1}{2} U_T c C_l \left(1 - \frac{C_d}{C_l \tan\phi}\right), \tag{11}$$

where c is the chord, C_l and C_d are the lift and drag coefficients, respectively, and the total blade element velocity is

$$U_T = \sqrt{\left(V_1 - u_{a,b}\right)^2 + \left(\Omega r + u_{c,b}\right)^2}, \tag{12}$$

where subscript "b" indicates, as before, the velocities are at the blades and not the streamtube averages.

For the development of BEMT for DAWTs, the important results of this section are Eqs. (11) and (12). p will also be shown to be dynamically important for reasons directly connected to the vortex geometry. For bare turbines, w is usually taken as a parameter that can be optimized to maximized turbine output power, e.g. [16], [19], and [22]. It has been found that $w \to 1/3$ as $\lambda \to \infty$, that is, the vortex sheet moves with the velocity of the remainder of the wake.

3. Blade Element Theory for DAWTs

The inclusion of F_u and F_w in the blade element equations for DAWTs is straightforward. Vaz & Wood [11] derived these equations, but they used F_P. All that is necessary here is to substitute F_u for F_P in the thrust equation and F_w for F_P in the torque equation. Eq. (16) of [11] gives the elemental thrust, C_T, and torque coefficients, C_M, on the blade elements intersecting an annular control volume at radius r, which hereinafter is normalized by R, as

$$\frac{dC_T}{dr} + \frac{dC_{Td}}{dr} = 4\varepsilon_1 \left(1 - \varepsilon_4\right) r, \tag{13}$$

where C_{Td} is the thrust coefficient of the diffuser, and ε_4 is the streamtube average diffuser exit velocity given by Eq. (18) of [11], and

$$\frac{dC_M}{dr} = 4\varepsilon_1 u_c r^2, \tag{14}$$

with the normalized velocity at the rotor plane ε_1 given by

$$\varepsilon_1 = V_1 \left(1 - a\right) / V_0 = (1 + v_d)(1 - a), \tag{15}$$

where a, the streamtube average axial induction factor, is defined in the same way as for a bare turbine, as V_1 would be the velocity at the location of the rotor if it was removed. After the change from using F_P to F_u and F_w, Eq. (15) is the main difference from the analysis of [11]. ε_4 is given by

$$\varepsilon_4 = \varepsilon_{1,b} - \sqrt{(1-\varepsilon_{1,b})^2 + C_{Td} - \varepsilon_{1,b}^2(1-\beta^2)(1-\eta_d)}. \tag{16}$$

with $\varepsilon_{1,b} = (1+v_d)\,(1-a_b F_u)$, and F_u replacing F_P. Combining Eqs. (13) and (16) gives

$$\frac{dC_T}{dr} + \frac{dC_{Td}}{dr} = 4\varepsilon_1 \left[1 - \varepsilon_{1,b} + \sqrt{(1-\varepsilon_{1,b})^2 + C_{Td} - \varepsilon_{1,b}^2(1-\beta^2)(1-\eta_d)}\right] r, \tag{17}$$

which is the new form of Eq. (19) of [11], and

$$\frac{dC_M}{dr} = 8a_b' F_w \lambda\,(1+v_d)\,(1-a_b)\,r^3, \tag{18}$$

where $\lambda = \Omega R/V_0$ is the conventional tip speed ratio. This is the new form of Eq. (20) of [11]. Note that for a bare turbine ($\eta_d = 1$ and $C_{Td} = 0$), Eq (17) reduces to Eq. (5) of Wood & Okulov [19], while Eq. (18) matches their (6), when the missing λr is included in the latter. The element power is obtained from

$$dP = \Omega dM = 4\rho a_b' F_w V_0\,(1+v_d)\,(1-a_b)\Omega^2 r^3 \pi dr. \tag{19}$$

By integrating this expression across the rotor, the power coefficient is given by

$$C_P = \frac{P}{\frac{1}{2}\rho A V_0^3} = \frac{8\,(1+v_d)}{\lambda^2} \int_0^\lambda a_b' F_w (1-a_b) x^3 dx, \tag{20}$$

where $x = \Omega r/V_0$ is the local-speed ratio.

From the lift and drag acting on an element, the contributions to the thrust and torque coefficients are

$$\frac{dC_T}{dr} = 2\left[(1+v_d)\,(1-a_b)\right]^2 \frac{\sigma C_n r}{\sin^2\phi} \tag{21}$$

and

$$\frac{dC_M}{dr} = 2\frac{(1+v_d)\,(1-a_b)\,(1+a'_b)\,\sigma C_t \lambda r^3}{\sin\phi\cos\phi}, \tag{22}$$

where $\sigma = Nc/(2\pi r)$ is the local solidity. The elemental normal and tangential force coefficients C_n and C_t, respectively, at any r have the same definition as for a bare turbine, see Eqs. (16) and (17) of Vaz & Wood [26]. C_n and C_t are a convenient way of using the element lift and drag coefficients. The flow angle, ϕ, is given by Eq. (25) of Vaz & Wood [11]. An extended formulation for the axial and tangential flow velocities can be obtained by combining Eqs. (17) and (18) with Eqs. (21) and (22) respectively, yielding

$$1-\varepsilon_{1,b}+\sqrt{(1-\varepsilon_{1,b})^2+C_{Td}-\varepsilon_{1,b}^2(1-\beta^2)(1-\eta_d)}-\frac{1}{4\varepsilon_1 r}\frac{dC_{Td}}{dr}=\frac{\varepsilon_1\sigma C_n}{2\sin^2\phi} \tag{23}$$

and

$$\frac{a'_b}{1+a'_b}=\frac{\sigma C_t}{4F_w\sin\phi\cos\phi}. \tag{24}$$

Section 4 describes the calculation of F_u and F_w.

3.1. Blade Element Optimization for DAWTs

The optimum value of ε_{1opt} is determined by maximizing C_P according to the description in [11], which is done using

$$6\varepsilon_{1opt}^3\left[\beta^2(1-\eta_d)+\eta_d\right]-C_{Td}\Delta+4\varepsilon_{1opt}(1+C_{Td}+\Delta)-2\varepsilon_{1opt}^2(5+3\Delta)=0, \tag{25}$$

where

$$\Delta=\sqrt{1+C_{Td}+\varepsilon_{1opt}\left\{-2+\varepsilon_{1opt}\left[\beta^2(1-\eta_d)+\eta_d\right]\right\}}. \tag{26}$$

which are Eqs. (29) and (3) of [11]. Once ε_{1opt} is obtained, the optimized a_{opt} may be easily calculated through $a_{bopt} = 1-\varepsilon_{1opt}$. a' as a function of ε_{1opt} is found using conservation of energy, resulting in optimum element power:

$$dP_{opt}=\frac{1}{2}\rho V_0^3\left[\varepsilon_{1opt}\left(1-\varepsilon_{4opt}^2\right)-\varepsilon_{1opt}^2\left(1-\beta^2\right)(1-\eta_d)\right]dA. \tag{27}$$

Also, applying the angular momentum equation at a blade section,

$$dP_{opt} = 2\rho V_0 a'_b \varepsilon_{1opt} \Omega^2 r^2 dA. \tag{28}$$

Equating (27) and (28) gives

$$a'_{bopt} = \frac{2\varepsilon_{1opt}\left(1-\varepsilon_{4opt}\right) - C_{Td}}{4x^2}, \tag{29}$$

with ε_{4opt} given by

$$\varepsilon_{4opt} = \varepsilon_{1opt} - \sqrt{\left(1-\varepsilon_{1opt}\right)^2 + C_{Td} - \varepsilon_{1opt}^2(1-\beta^2)(1-\eta_d)}. \tag{30}$$

In this case, F_u is included in ε_{4opt} through $\varepsilon_{1opt} = (1+v_d)(1-a_{bopt}F_u)$. Hence, the optimum flow angle, ϕ_{opt}, can be determined through

$$\phi_{opt} = \tan^{-1}\left[\frac{(1+v_d)(1-a_{bopt})}{x(1+a'_{bopt})}\right]. \tag{31}$$

To calculate the optimum twist angle, θ_{opt}, and chord, c_{opt}, the following expressions are used:

$$\theta_{opt} = \phi_{opt} - \alpha_{opt} \tag{32}$$

and

$$c_{opt} = 4\pi r\left(1-\varepsilon_{4opt}\right)\frac{\sin^2(\phi)}{NC_n\varepsilon_{1opt}}. \tag{33}$$

Note that Eq. (33) comes directly from (21).

4. Calculation of the Finite Blade Functions for DAWTs

The procedure developed in [16], [17], and [19] calculates the mean induced velocities from their simple dependence on Γ, given by Eq. (11). The major difference is that Γ and $p(r)$ are calculated through BEMT expressions, which are dependent on η_d, β, and C_{Td}. Thus, for the streamtube whose centre is at radius r, a and a' in Eq. (1) are given by

$$a = \frac{N\Gamma}{4\pi p V_0} \quad \text{and} \quad a' = \frac{W}{\Omega r} = \frac{N\Gamma}{4\Omega\pi r^2}, \tag{34}$$

where W is the induced circumferential velocity. Note that the terms involving Γ are consistent with Eqs. (8) and (9). Further

$$a_b = a + \delta a \quad \text{and} \quad a'_b = a' + \delta a', \tag{35}$$

where δa and $\delta a'$, the difference between the values at the blades and the means, are due entirely to the trailing vortices. They are found using Okulov's approximation to the KH equations. The BEMT implementation of these equations, including the use of Kawada cancellation, is described in Section 2 of Wood [16], especially Eqs. (6) and (7), so the details will be omitted here. The only significant alteration to that method is including η_d, β, and C_{Td} in F_u and F_w through Eqs. (11) and (36). The finite blade functions are then computed using Eq. (1). The presence of η_d, β, and C_{Td} in the calculation of U, W, and the values at the blade requires F_u and F_w to remain finite at the blade tip unless $v_d = 0$ for a bare turbine.

The final requirement is a value of p. Following [17], [19], and [16], this is given by

$$p = dC_M/dC_T, \tag{36}$$

and so it is easily obtained from Eqs. (21) and (22). The use of Eq. (36) removes the need to compute an optimum w for the vortex sheet in Eq. (7).

The iterative algorithm for the calculation of optimum chord and twist angle, starting at the tip, is described below, using the following as input: r, η_d, β, C_{Td}, $C_L(\alpha_{opt})$, $C_D(\alpha_{opt})$ and V_0 for a given λ. Note that there are two iterations over N_s, the number of blade sections: the first is the blade element calculations and the second is to determine F_u and F_w. Conventional BEMT algorithms use only the first. For all calculations in this paper, $N_s = 30$.

Set initial values: $F_u = F_w = 1$;
while $error > TOL$ **do**
  for $i = 1$ to N_s **do**
    $iter = iter + 1$;
    Compute a_{bopt}, making $a_{bopt} = 1 - \varepsilon_{1opt}$ using Eq. (25), and a'_{bopt} using Eq. (29);
    Compute ϕ_{opt} using Eq. (31);
    Compute $C_n = C_L(\alpha_{opt})\cos\phi_{opt} + C_D(\alpha_{opt})\sin\phi_{opt}$ and $C_t = C_L(\alpha_{opt})\sin\phi_{opt} - C_D(\alpha_{opt})\cos\phi_{opt}$, respectively, where α_{opt} is obtained from maximum C_L/C_D;
    Compute θ_{opt} and c_{opt}, using Eqs. (32) and (33), respectively;
    Compute U_T using Eq. (12);
    Compute dC_T and dC_M using Eqs. (17) and (18), respectively;
  end for
  Compute $C_p = \lambda \sum dC_M$;
  Compute Γ using Eq. (11);
  Compute p using Eq. (36);
  for $i = 1$ to N_s **do**
    Compute new $F_u = a/a_{bopt}$ and new $F_w = a'/a'_{bopt}$ using Eq. (34). It is important to note that F_u and F_w are implemented in the algorithm through $\varepsilon_{1,b} = (1 + v_d)(1 - a_b F_u)$, and F_w in Eq. (18);
  end for
  Compute $error = \left| C_p^{iter+1} - C_p^{iter} \right|$.
end while
Compute blade geometry.

5. The Simulated Diffuser-Augmented Wind Turbine

We consider the diffuser of Hansen et al. [2], made by deforming the NACA 0015 airfoil, for which the parameters are shown in Table 1. To evaluate F_u and F_w, it is necessary to find v_d through Eq. (5). The difference for v_d between the present model and the CFD results of Hansen et al. [2] is about 0.012%, for the same values for β, η_d, and c_{p3}. This implies the validity of Eq. (5) for the induced velocity, v_d.

Table 1: Comparison between the proposed model and CFD [2].

	β	η_d	c_{p3}	v_d
Hansen et al. [2]	0.54	0.83	-0.38	0.83
Present work, Eq. (5)	0.54	0.83	-0.38	0.8301

A DAWT optimization was done for $N = 3$ using the symmetrical NACA 0012 airfoil, with C_l and C_d obtained experimentally by Sheldahl and Klimas [50]. The main parameters for the optimization procedure are shown in Table 2. The NACA 0012 is one of the most studied airfoils, so there are extensive experimental data available in the literature. The NACA 0012 airfoil is used here for convenience: it is not the objective of this work to evaluate the effect of the airfoil on DAWT performance. The angle of attack of 8° gave the maximum C_l/C_d around 44, for a Reynolds number of 1.6×10^5. The parameters listed in Table 2 are input data for the present procedure, through which the blade is designed. In the optimization, F_u and F_w are calculated from the contribution to the blade element velocities induced by the vortices trailing from each element junctions, as well as the hub and the tip.

Table 2: Design parameters used in the simulation of the DAWT.

Parameters	**Values**
Turbine Diameter (D)	2.0 m
Hub Diameter (d)	0.2 m
Lift coefficient (C_l)	0.8274
Drag coefficient (C_d)	0.0185
Optimum angle of attack (α)	8°
Number of blades (N)	3
Tip-Speed Ratio (λ)	2.0 and 7.0
Air density (ρ) at 25°C	1.2 kg/m^3

6. Results and Discussion

Fig. 4 shows the behavior of the finite blade functions, F_u, F_w, and F_p at $\lambda = 2.0$. For $v_d = 0.0$ (Fig. 4a), indicating that for a bare turbine, F_u and F_w are coincident, as they must be if p is constant, which is an optimality condition, e.g. Wood [16]. As in previous analyses, e.g. Wood [16], the

calculated F_u and F_w exceed unity near the hub. It is not clear whether this behaviour is correct, but, fortunately, the contribution to the power and thrust from the hub region is small. The finite blade functions, therefore, were constrained so that $F_u \leqslant 1$ and $F_w \leqslant 1$ along the entire blade. Thus, near the hub, F_u and F_w remain equal to unity with and without the diffuser, Fig. 4. Over the whole blade, F_u and F_w change substantially compared to F_p when there is a diffuser as shown in Fig. 4b. Also, $F_u > F_w$ close to the tip, where v_d becomes the dominant contribution to the streamtube average as well as the velocity at the blades. Such a behavior does not occur for F_p. Fig. 5 shows F_u, F_w, and F_P for $\lambda = 7.0$. Note that F_u, F_w and F_P are more nearly equal for the bare turbine (Fig. 5a). This occurs because F_P becomes more accurate as λ increases, as pointed out in [51]. For $v_d = 0.82$, indicating a DAWT with $C_{T,d} = 0.8$, F_u remains equals to F_w at this higher λ, but larger than F_p, as shown in Fig. 5b. As shown by the insert in Fig. 5b, $F_u \approx F_w$ at the tip, despite the diffuser contributing to the axial flow only. We interpret this result to mean that the blade bound circulation stays positive due to v_d and this causes F_w to be non-zero. The difference between F_P and F_u and F_w is further reflected in Fig. 6, which shows Γ, with and without the diffuser. Clearly, the diffuser increases the circulation along the entire blade, making $F_u = F_w > F_p$ when λ increases. This increase in circulation increases the power extraction, but it also may increase the effect of cavitation. This is a very important phenomenon for hydrokinetic turbine blade optimization, which is intensified when operating at low λ.

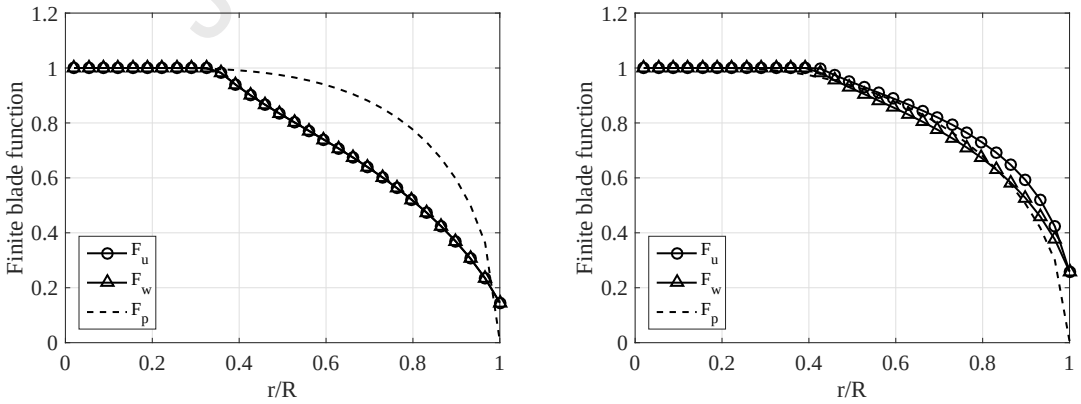

Figure 4: $\lambda = 2.0$: (a) $v_d = 0.0$ (b) $v_d = 0.82$.

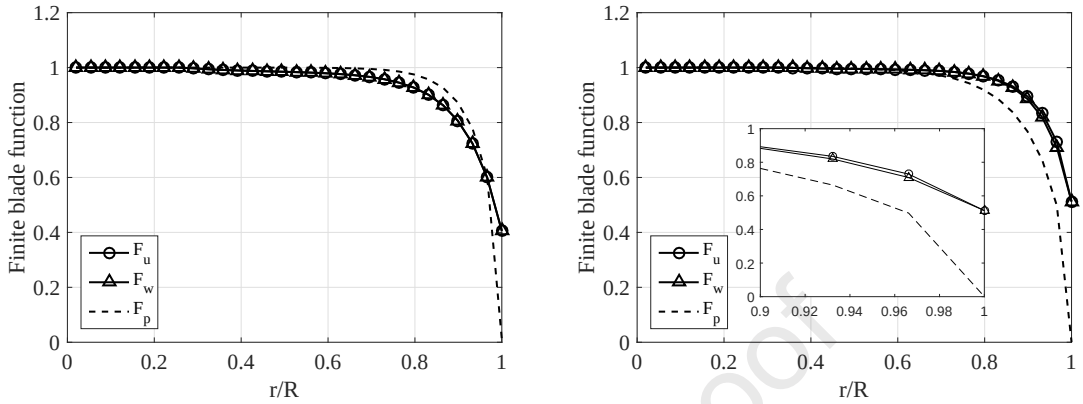

Figure 5: $\lambda = 7.0$: (a) $v_d = 0.0$ (b) $v_d = 0.82$.

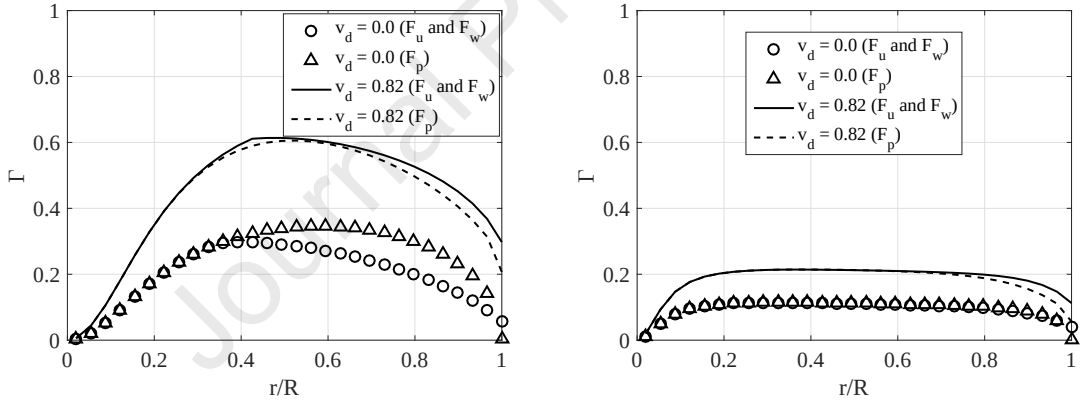

Figure 6: (a)$\lambda = 2.0$. (b) $\lambda = 7.0$.

We now discuss the effect of the finite blade functions on the optimal c and θ distributions, which depend on them through Eqs. (32) and (33). From the results of the previous section, we expect the impact of using F_u and F_w in relation to F_P to be greater at the lower λ. Fig. 7a shows the chord and twist angle distributions for $\lambda = 2.0$. Using F_u and F_w, even for the bare turbine, gives a very different distribution of c to that using F_P, while θ remains the same as for F_p, but sensitive to the diffuser as shown in Fig. 7b. At low λ, c from F_u and F_w is close to the Prandtl distribution,

being different only close to the blade tip. As the diffuser causes a finite v_d, c near the tip remains slightly larger when using the finite blade functions, agreeing with the result in Fig. 4b, where F_u and F_w are directly affected by v_d. For $\lambda = 7.0$, Fig. 8a, c and θ are the same as that obtained using F_P. Even with the diffuser, Fig. 8b, c and θ distributions are only slightly different very close to the blade tip, but all of them are very sensitive to the diffuser. The optimized power extraction is listed in Table 3; using F_u and F_w the power is almost equal that using F_p for $\lambda = 2.0$. However, for $\lambda = 7.0$ the power is about 6.6% higher than for F_p mainly because v_d increases F_u and F_w. These results demonstrate that to optimize DAWTs it is necessary to consider the axial induced velocity, v_d, of the diffuser, which alters the finite blade function mainly close to the tip.

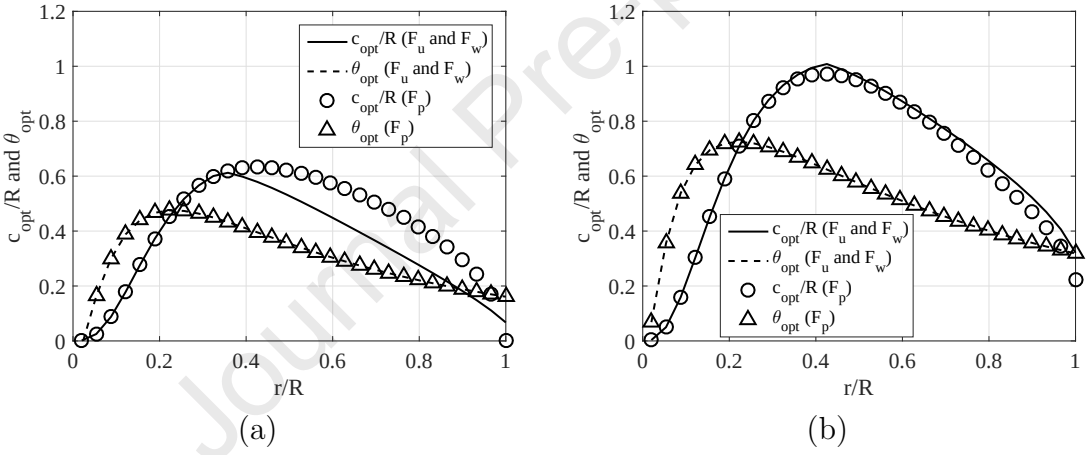

Figure 7: $\lambda = 2.0$: (a) $v_d = 0.0$ (b) $v_d = 0.82$.

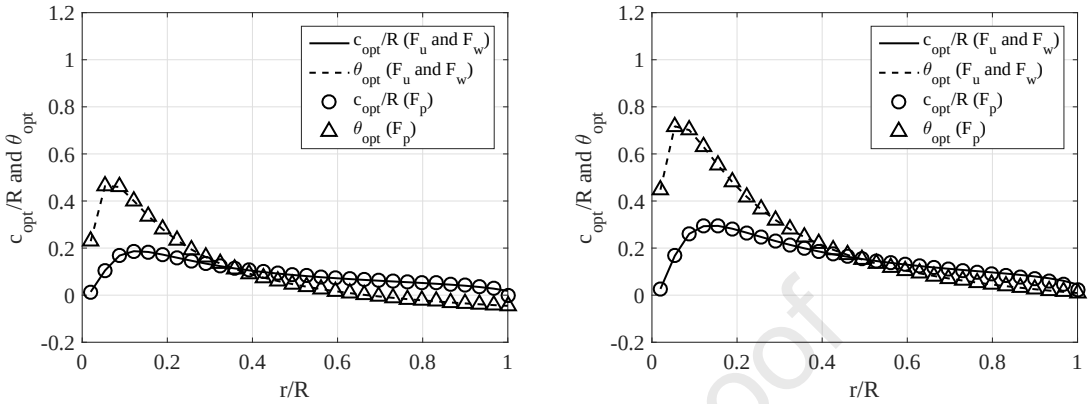

Figure 8: $\lambda = 7.0$: (a) $v_d = 0.0$ (b) $v_d = 0.82$.

Table 3: Comparison between optimized power coefficients ($v_d = 0.82$).

	$\lambda = 2.0$	$\lambda = 7.0$
C_P using F_p	0.63	0.76
C_P using F_u and F_w	0.64	0.81

We now compare the present analysis with the experimental data of Hoopen [48] for a 3-bladed DAWT of 1.5 m rotor diameter at $\lambda = 5.6$. [48] gives all parameters needed for the present simulation, making his work an important DAWT source. Table 4 shows the present results compared with Hoopen's measurements and other methods available in the literature. Note that the power output (530.04 W) obtained using F_u and F_w is close to the experimental value (531 W), while using F_p the difference is slightly larger. The same occurs with the turbine torque. The thrust on the rotor using F_u and F_w also shows good agreement with the measurements, as well as that value using F_p. Fig. 9a shows the behavior of F_u, F_w, and F_p for $V_0 = 10$ m/s. As $\lambda = 5.6$ in this case, F_u, F_w, and F_p are almost the same. Fig. 9b shows the augmentation factor, A_f, in relation to the wind velocity, V_0. A_f is defined in [11]; $A_f = 27\eta_t/16$, with $\eta_t = \eta_p \eta_g C_P$, where $\eta_p = 0.85$ is the drivetrain efficiency and $\eta_g = 0.74$ is the generator efficiency. The results in Fig. 9 were obtained for constant Ω, so $\lambda = 56/V_0$. Clearly, the results using F_u and F_w, and also F_p are consistent with the measurements. This occurs because to calculate F_u, F_w, and F_p it is necessary to include v_d in the

BEMT calculations. As before, the differences between F_P and F_u and F_w increase with decreasing λ. For the results in Fig. 9, $v_d = 0.85$, which was calculated for $c_{p3} = -0.49$, $\beta = 0.5785$ and $C_{Td} = 0.135$ as described in [48].

Fig. 9b suggest the intriguing possibility that maximum DAWT and DAHKT performance is much less dependent on λ than for a bare turbine. This would allow consideration of factors other than the maximization of power in turbine design. These other factors include: high λ performance usually allows more efficient and cheaper generators, but lower λ is likely to reduce cavitation in DAHKTs and the lower blade rotation would reduce the likelihood of damage to fish and other river life. Further, the high c/R shown in Fig. 7 implies high solidity and possibly higher lift:drag on the blade elements.

Table 4: Comparison between the present study and experimental data ($V_0 = 10m/s$).

	Angular speed (rad/s)	Power output (W)	Torque (Nm)	Thrust coefficient
Experimental [48]	75	531.00	7.10	0.80
Rio Vaz et al. [32]	75	526.00	6.10	-
Present work using F_p	75	536.26	7.15	0.77
Present work using F_u and F_w	75	530.04	7.07	0.77
CFD [48]	137	545.00	4.00	-
CFD [48]	155	246.00	1.60	-

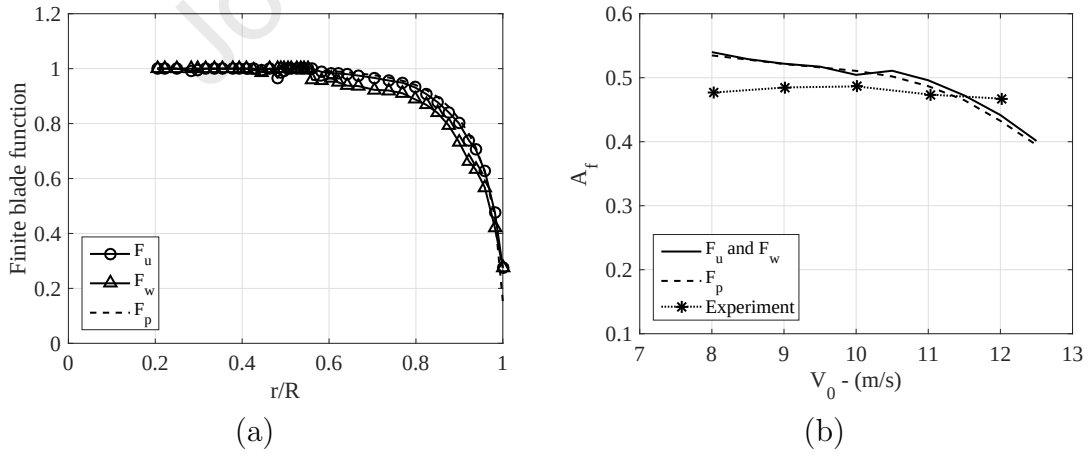

Figure 9: (a) Finite blade functions in relation to the radial position for $V_0 = 10$ m/s. (b) Augmentation factor in relation to V_0 (experiment obtained from [48]).

7. Conclusions

The present study considered an issue in blade element modeling of diffuser augmented wind and hydrokinetic turbines that has not received sufficient attention: the effects of the finite number of blades on the turbine power and thrust. These are usually modeled by Prandtl's well-known tip loss factor which asymptotes to zero at the blade tip. The diffuser, however, induces an additional flow through the rotor causing finite blade loading at the tip. Finite blade effects are measured by the ratio of the velocity at the blade to the streamtube average. A diffuser has equal effect on the axial velocities, so their ratio cannot reach zero. There is no corresponding constraint on the circumferential velocity, but F_w as well as F_u was found not to go to zero at the tip.

F_u and F_w were modeled using a simple modification of the analysis of Wood & Okulov [16] and Wood [19] for bare turbines to determine the finite blade functions for the axial and circumferential velocities. As it is not clear whether F_u and F_w can exceed unity, we limited the calculated values to unity. This had only a small effect on the analysis because the exceedence occurred only near the hub. The new analysis gave 6% increased power for a computationally-optimized blade at the higher value of tip speed ratio of the two that were analyzed.

By comparison to the limited experimental data for a diffuser-augmented wind turbine, we could not distinguish between F_P and F_u and F_w in terms of accuracy, as shown in Tab. 4. In addition, this work suggests that diffuser-augmented wind turbines have much flatter power curves than bare turbines. Some of the possible advantages of this behaviour were given. These results show that the new finite blade functions can be implemented in BEMT analysis, in order to contribute for a more accurate BEMT model for DAWTs.

Nomenclature

Latin Symbols

a, a'	Streamtube average axial and tangential induction factors
a_b, a'_b	Axial and tangential induction factors at the blade
A, A_3	Area of the disc and the cross section at the diffuser outlet
B	Number of blades
c	Chord (m)
C_D	Drag coefficient
C_L	Lift coefficient
C_M	Torque coefficient
C_n	Normal force coefficient
c_{p3}	Pressure coefficient at the diffuser outlet
C_P	Power coefficient
C_t	Tangential force coefficient
C_T	Thrust coefficient
C_{Td}	Diffuser thrust coefficient
dM	Elementary torque (Nm)
dP	Elementary power (W)
F	Prandtl Tip-loss factor
F_u, F_w	Finite blade functions for axial and circumferential flow, respectively
H	Losses through the diffuser in terms of pressure (Pa)
p_0	Pressure in the external flow (Pa)
p_2	Pressure at the turbine upstream (Pa)
p_3	Pressure at the diffuser outlet (Pa)
P	Power output (W)
Q	Flow rate (m^3/s)
r	Radial position at the rotor plane (m)
R	Radius of the rotor (m)
T	Thrust of the rotor (N)
T_d	Thrust of the diffuser (N)
u_θ	Swirl velocity in the near wake (m/s)
V_0	Freestream wind velocity (m/s)
V_1, V_2	Axial velocity at the rotor (m/s)
V_3	Axial velocity at the diffuser outlet (m/s)
V_4	Axial velocity in the wake (m/s)
x	Local-speed ratio

Greek Symbols

α	Angle of attack (rad)
β	Area ratio
ε_1	Velocity ratio
ε_4	Far-wake velocity ratio
η_d	Diffuser efficiency
θ	Twist angle (rad)
λ	Tip-speed ratio

Acknowledgments

The contribution of VLO and DHW was supported by a contract with the Ministry of Education and Science of the Russian Federation (no. 075-15-2019-1923). JRPV thanks CNPq, CAPES, PROCAD project (no. 88881.200549/2018-01), and PROPESP/UFPA for financial support.

[1] Jamieson, P. Innovation in wind turbine design. John Wiley & Sons, 2018.

[2] Hansen, M.O.L.; Sorensen, N.N.; Flay, R.G.J. Effect of placing a diffuser around a wind turbine. Wind Energy 2000; 3:207-213

[3] Hjort, S., Larsen, H. . A multi-element diffuser augmented wind turbine. Energies 2015 7(5): 3256-3281.

[4] Anup, K. C., Whale, J., Urmee, T. Urban wind conditions and small wind turbines in the built environment: A review. Renewable Energy 2018, 131:268-283.

[5] Dilimulati, A., Stathopoulos, T., Paraschivoiu, M. Wind turbine designs for urban applications: A case study of shrouded diffuser casing for turbines. Journal of Wind Engineering and Industrial Aerodynamics 2018, 175: 179-192.

[6] Silva, P. A., Vaz, D. A. R., Britto, V., de Oliveira, T. F., Vaz, J. R., Junior, A. C. B. A new approach for the design of diffuser-augmented hydro turbines using the blade element momentum. Energy Conversion and Management, 2018, 165, 801-814.

[7] Lubitz, W.D., Shomer, A. Wind loads and efficiency of a diffuser augmented wind turbine, Proc. CSME Intl Congress, Toronto, 2014.

[8] Hansen, M.O.L., The Aerodynamics of Wind Turbines, 2nd edn, Earthscan.

[9] Kesby, J. E., D. R. Bradney, P. D. Clausen. Determining Diffuser Augmented Wind Turbine performance using a combined CFD/BEM method. Journal of Physics: Conference Series. 753(8). IOP Publishing, 2016.

[10] Fletcher, C.A.J. Computational analysis of diffuser-augmented wind turbines. Energy Conversion Management 1981; 21:175-183.

[11] Vaz, J.R.P., Wood, D.H., Effect of the diffuser efficiency on wind turbine performance. Renewable Energy 2018, 126:969-977.

[12] Glauert H. Aerodynamic theory. In: Durand WF, editor. Chapter XI. Division L. Airplanes Propellers, vol.4; 1935. p.191-195 [reprinted, Dover, New York, 1963].

[13] Sørensen, J. N. General Momentum Theory for Horizontal Axis Wind Turbines. Research Topics in Wind Energy, Vol. 4, Springer International Publishing, 2016 (DOI 10.1007/978-3-319-22114-4).

[14] Shen, W.Z., Mikkelsen, R., Sørensen, J.N., Bak, C..Tip vortex corrections for wind turbine computations. Wind Energy 2005, 8:457-475.

[15] Wimhurst, A., and Willden, R. H. J.. Analysis of a tip correction factor for horizontal axis turbines. Wind Energy 2017, 20,1515-1528.

[16] Wood, D. H. Application of extended vortex theory for blade element analysis of horizontal-axis wind turbines. Renewable Energy 2018, 121: 188-194.

[17] Wood, D. H. A cascade model of blade element interaction for wind turbines with unequal blades. International Journal of Sustainable Energy, 2016, 35(5): 502-512.

[18] Passmann M, aus der Wiesche S, Joos F. An Experimental and Numerical Study of Tip-Leakage Flows in an Idealized Turbine Tip Gap at High Mach Numbers. In Turbo Expo: Power for Land, Sea, and Air, 2018, 51005, V02BT41A023. American Society of Mechanical Engineers.

[19] Wood, D.H., Okulov, V.L., Nonlinear blade element-momentum analysis of Betz-Goldstein rotors, Renewable Energy 2017, 107:542-549.

[20] Okulov, V. L. On the stability of multiple helical vortices. Journal of Fluid Mechanics 2004, 521: 319-342.

[21] Fukumoto, Y., Okulov, V. L., Wood, D. H. . The contribution of Kawada to the analytical solution for the velocity induced by a helical vortex filament. Applied Mechanics Reviews 2015, 67(6): 060801.

[22] Okulov, V.L., Sørensen, J.N., Refined Betz limit for rotors with a finite number of blades. Wind Energy 2008, 11(4): 415-426.

[23] Sorribes-Palmer, F., Sanz-Andres, A., Ayuso, L., Sant, R., Franchini, S., Mixed CFD-1D wind turbine diffuser design optimization, Renewable Energy 2017, 105:386-399.

[24] Kosasih, B., Hudin, H.S., Influence of inflow turbulence intensity on the performance of bare and diffuser-augmented micro wind turbine model, Renewable Energy 2016, 87:154-167.

[25] Bontempo, R., Manna, M., Performance analysis of open and ducted wind turbines, Applied Energy 2014, 136:405-416.

[26] Vaz, J.R.P., Wood, D.H., Aerodynamic optimization of the blades of diffuser-augmented wind turbines. Energy Conversion and Management 2016, 123:35-45.

[27] Al-Sulaiman, F. A., Yilbas, B. S., Thermoeconomic analysis of shrouded wind turbines, Energy Conversion and Management 2015, 96:599-604.

[28] Jafari, S.A.H., Kosasih, B., Flow analysis of shrouded small wind turbine with a simple frustum diffuser with computational fluid dynamics simulations, Journal of Wind Engineering and Industrial Aerodynamics 2014, 125:102-110.

[29] Wang, W.X., Matsubara, T., Hu, J., Odahara, S., Nagai, T., Karasutani, T., Ohya, Y., Experimental investigation into the influence of the flanged diffuser on the dynamic behavior of CFRP blade of a shrouded wind turbine, Renewable Energy 2015, 78:386-397.

[30] Abe, K.; Ohya, Y. An investigation of flow fields around flanged diffusers using CFD, Journal of Wind Engineering Industrial Aerodynamics 2004;. 92: 315-330.

[31] Ohya, Y.; Karasudani, T. A shrouded wind turbine generating high output power with wind-lens technology, Energies 2010; 3:634-649.

[32] Rio Vaz, D. A. T. D., Mesquita, A. L. A., Vaz, J. R. P., Blanco, C. J. C., Pinho, J. T., An extension of the Blade Element Momentum method applied to Diffuser Augmented Wind Turbines, Energy Conversion and Management 2014, 87:1116-1123.

[33] Igra, O. Research and development for shrouded wind turbines. Energy Conversion Management 1981; 21: 13-48.

[34] Batchelor, G.K. An Introduction to Fluid Dynamics, C.U.P., 1967.

[35] Clausen, P.D., Koh, S.G., and Wood, D.H. (1993). Measurements of a turbulent boundary layer developing in a conical diffuser, Experimental Thermal and Fluid Science, 1993, 6: 39 - 48.

[36] Spera, D. A. Wind Turbine Technology: fundamental concepts of wind turbine engineering. ASME Press, 2nd Ed., New York, 2009.

[37] Wilson, R. E., and S. N. Walker, Performance Analysis of Horizontal Axis Wind Turbines, Corvallis 1984, Oregon: Oregon State University.

[38] Moriarty P.J., Hansen A.C. Aerodyn theory manual. Tech. Rep. NREL/TP 500-36881. Golden, CO: National Renewable Energy Laboratory; 2005.

[39] van Bussel, G.J.W. An assessment of the performance of diffuser augmented wind turbines (DAWT's). 3th ASME/JSME Joint Fluids Engineering Conference, July 18-23, San Francisco, California, USA; 1999.

[40] Phillips, D.G. An investigation on diffuser augmented wind turbine design, PhD. thesis, Department of Mechanical Engineering, School of Engineering, The University of Auckland; 2003.

[41] Hansen, M. Aerodynamics of wind turbines. Earthscan 2nd ed.; 2008.

[42] Wilson, R. E., Lissaman, P. B. S. Applied Aerodynamics of Wind Power Machines, Corvallis, Oregon: Oregon State University, 1974.

[43] Clifton-Smith, M. J., Wind Turbine Blade Optimisation with Tip Loss Corrections,Wind Engineering, 2009, 33(5):477496.

[44] Buhl, M. L., A New Empirical Relationship Between Thrust Coefficient and Induction Factor for the Turbulent Windmill State, Technical Report NREL/TP-500-36834, August 2005.

[45] Lock, C.N.H.; Batemen, H.; Townsend, H.C.H. (1926). An Extension of the Vortex Theory of Airscrews with Applications to Airscrews of Small Pitch, Including Experimental Results. No. 1014. Aeronautical Research

Committee Reports and Memoranda, London: Her Majesty's Stationery Office.

[46] Barbosa, D.L.M., Vaz, J.R.P., Figueiredo, S.W.O., Silva, M.O., Lins, E.F., Mesquita, A.L.A, An Investigation of a Mathematical Model for the Internal Velocity Profile of Conical Diffusers Applied to DAWTs, Annals of the Brazilian Academy of Sciences 2015, Vol. 87, No. 2, http://dx.doi.org/10.1590/0001-3765201520140114.

[47] Bontempo, R., Manna, M., Effects of the duct thrust on the performance of ducted wind turbines, Energy, 2016, 99:274-287.

[48] Hoopen P. D. C. An experimental and computational investigation of a diffuser augmented wind turbine: with an application of vortex generators on the diffuser trailing edge, M.Sc. Thesis. Faculty of Aerospace Engineering, Delft University of Technology; 2009.

[49] National Aerospace Laboratory (NLR). Evaluatie en verbetering van de prestaties van eenkleinschalige diffuser augmented wind turbine (DAWT); 1e fase; 2008.

[50] Sheldahl R, Klimas P. Aerodynamic characteristics of seven symmetrical airfoil sections through 180-degree angle of attack for use in aerodynamic analysis of vertical axis wind turbines. Sandia National Laboratories; 1981. Report SAND80-2114.

[51] Wood, D.H., Okulov, V.L. , Bhattacharjee, D., Direct calculation of wind turbine tip loss, Renewable Energy 2016, 95:269-276.

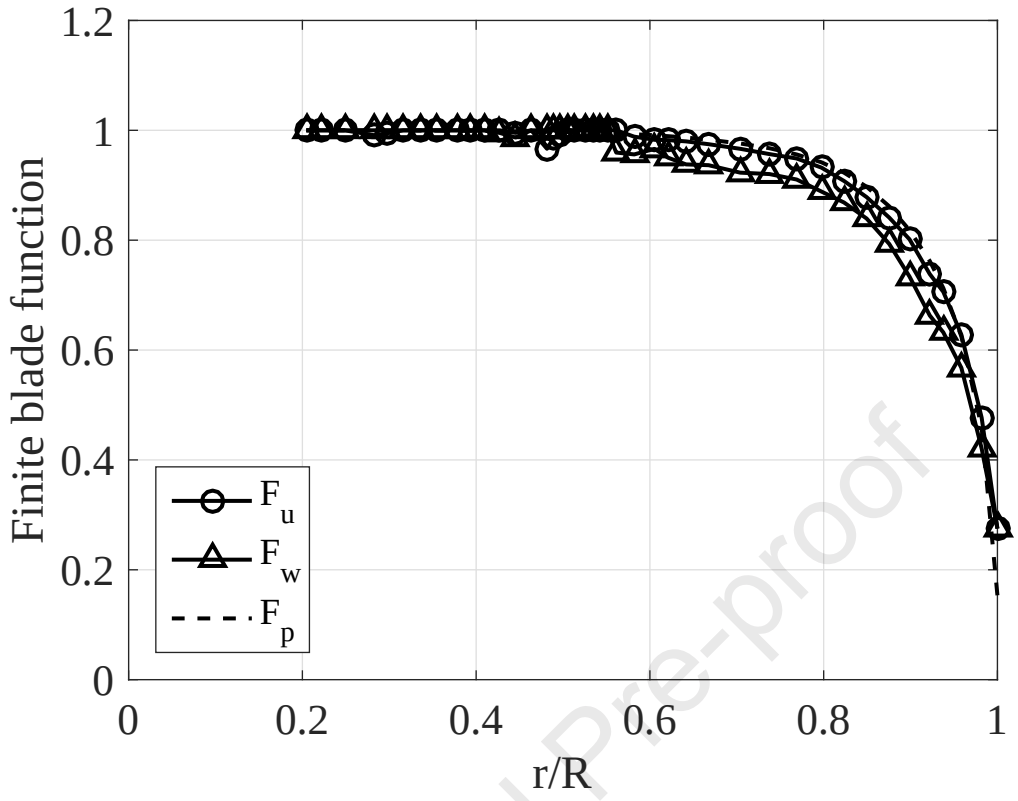

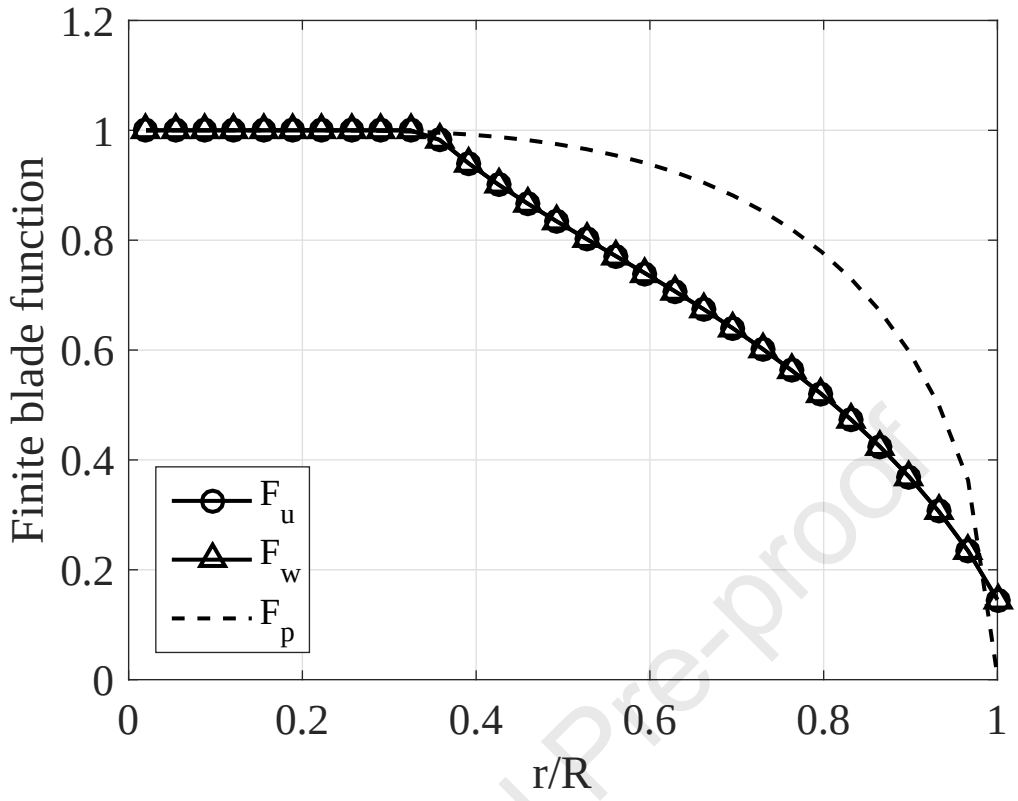

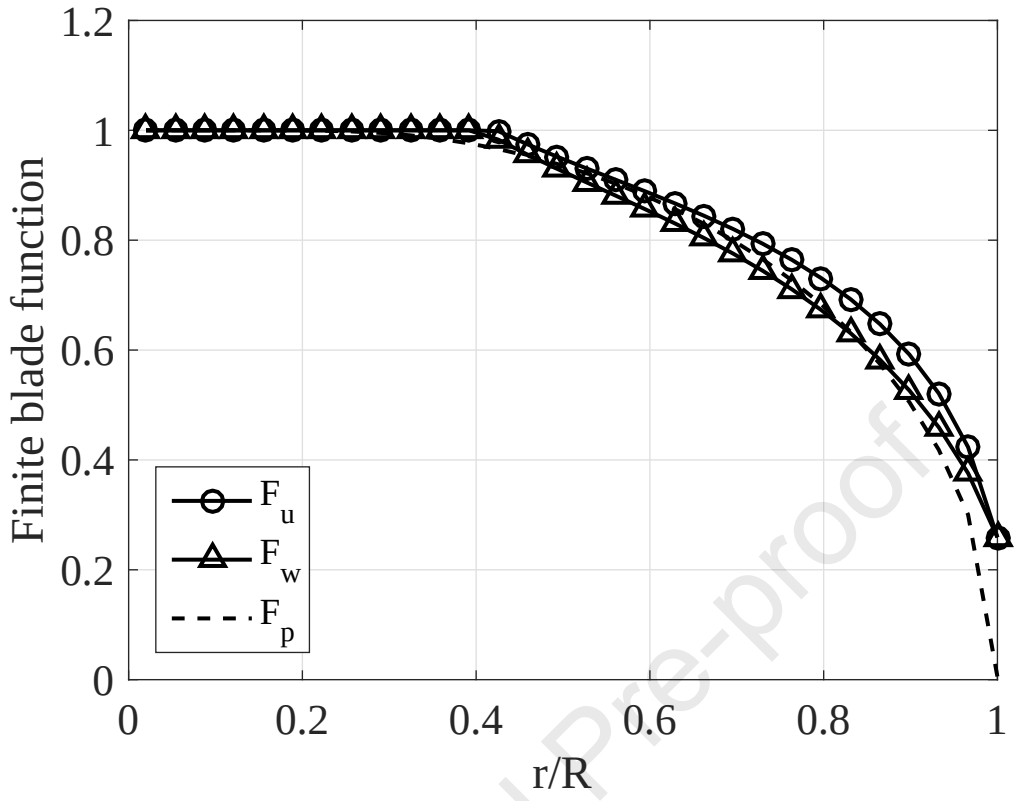

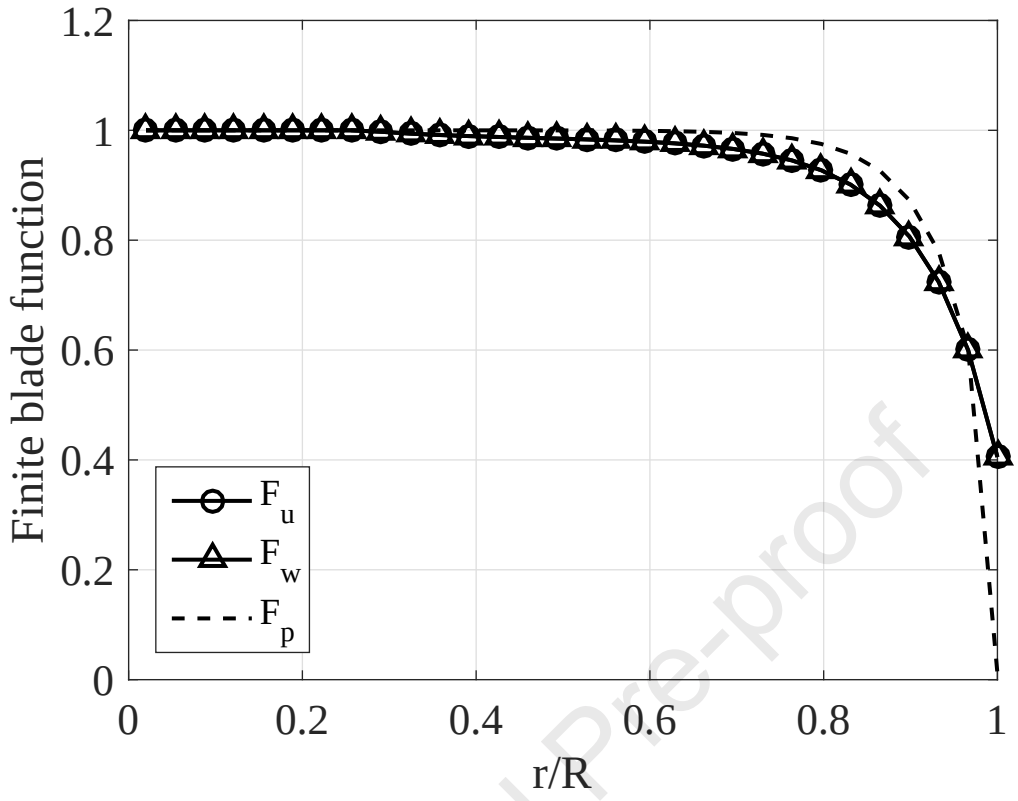

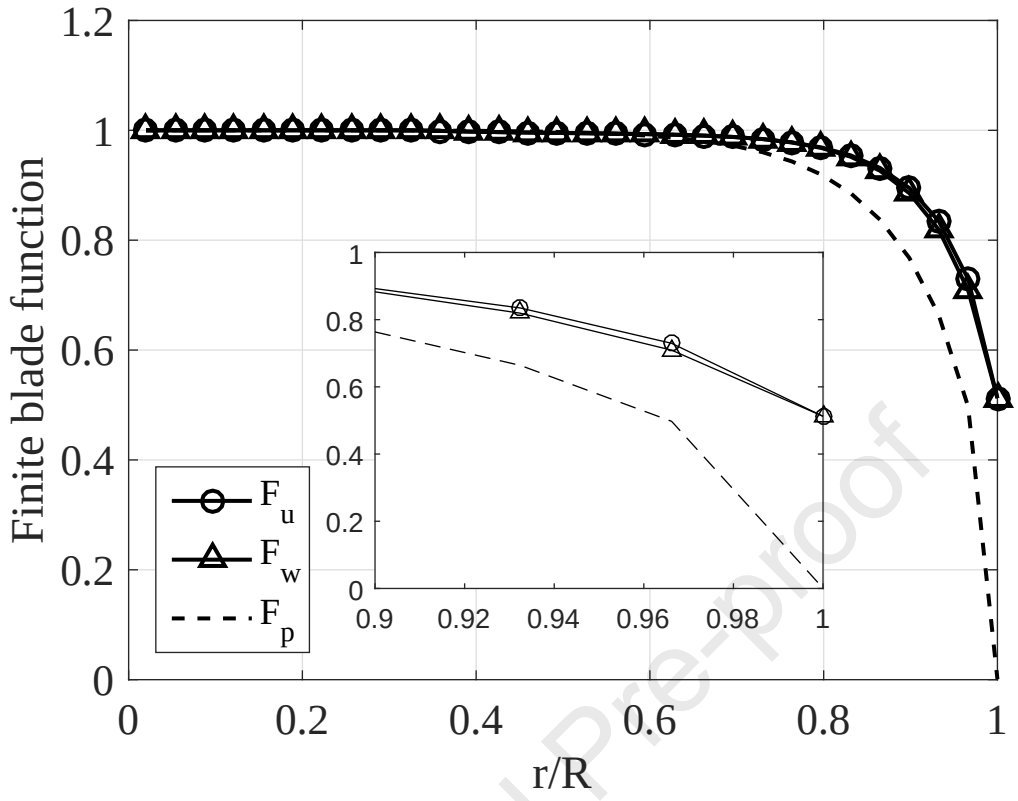

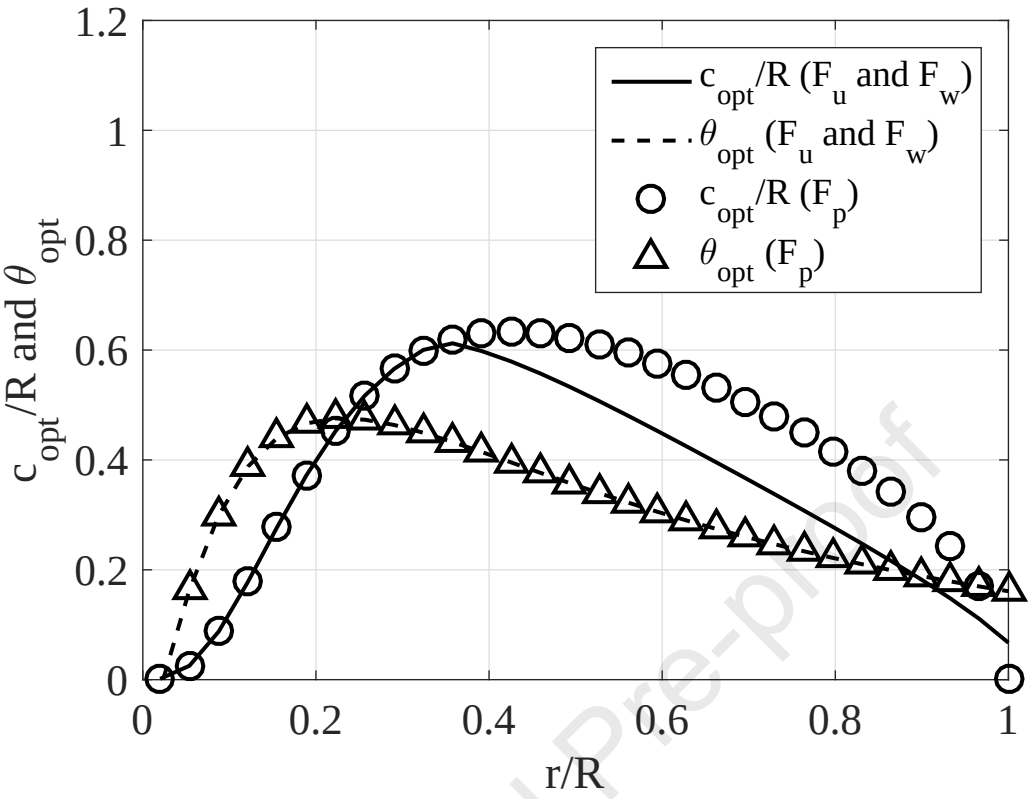

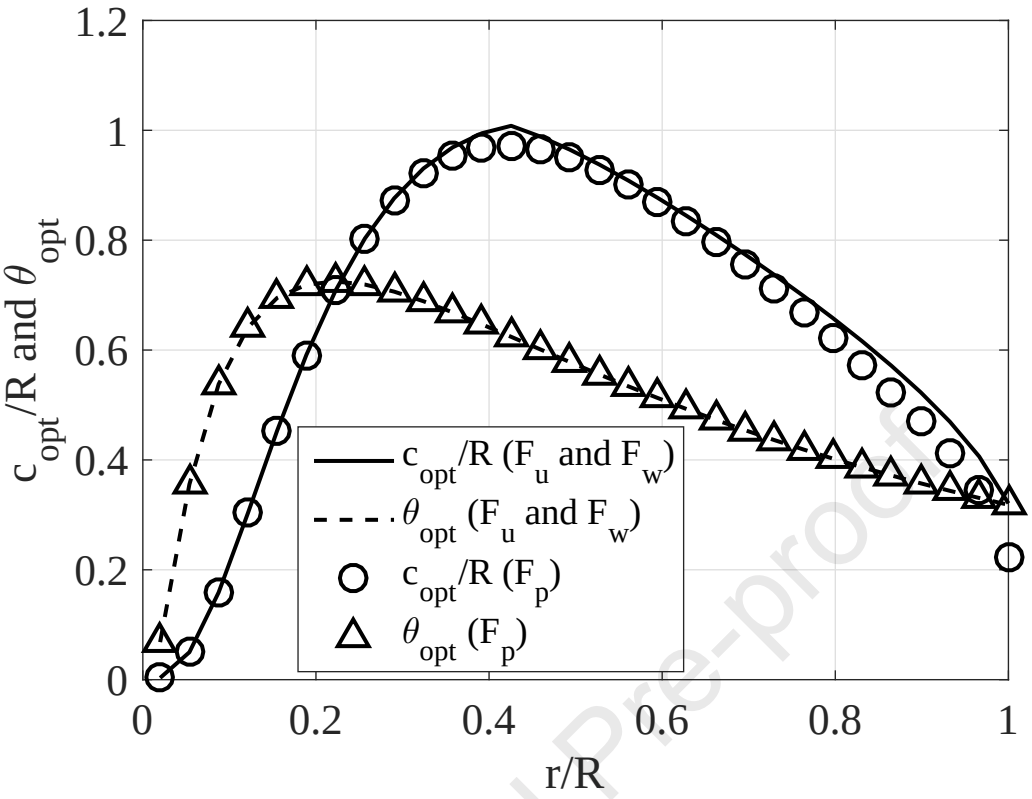

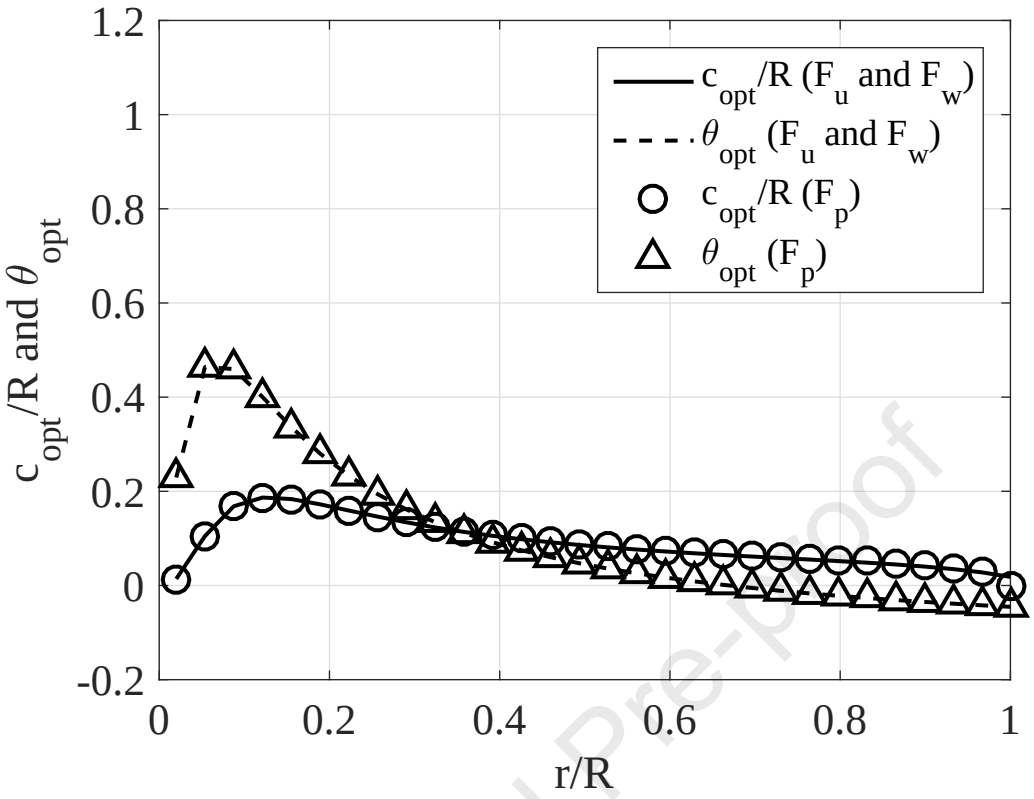

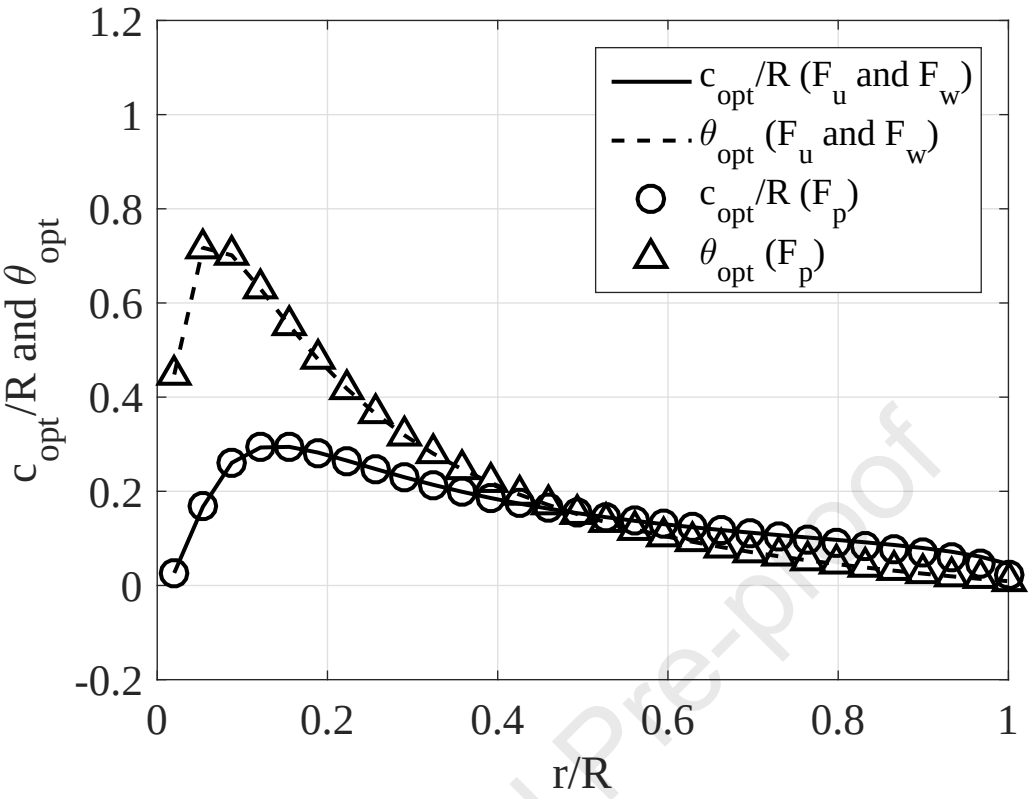

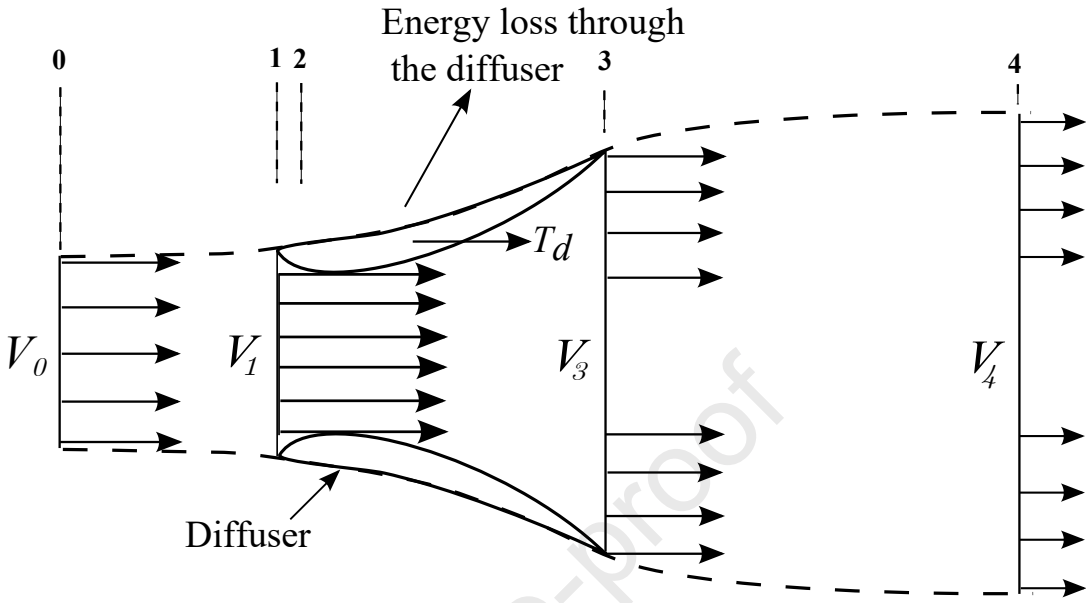

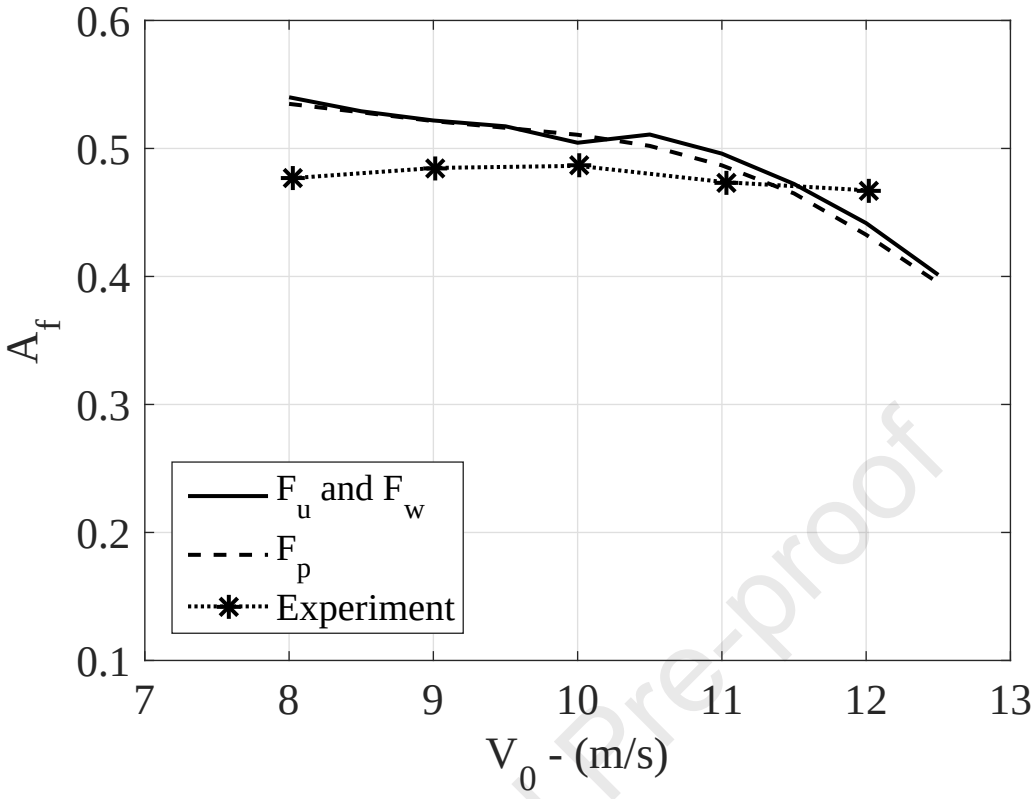

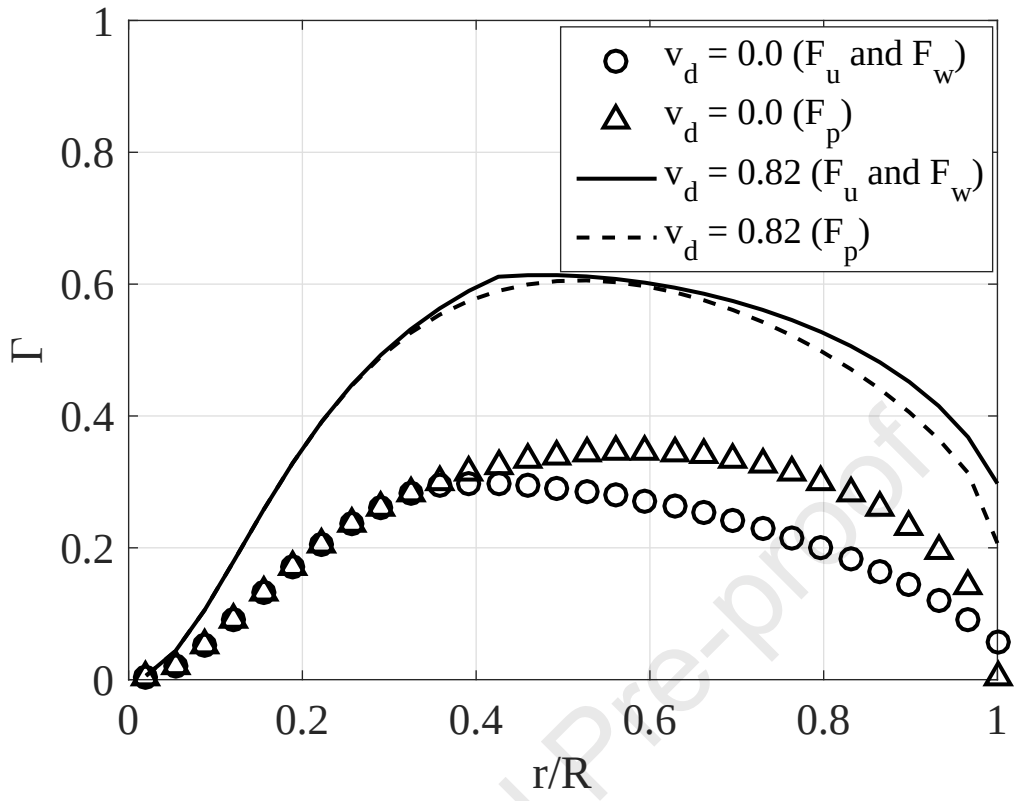

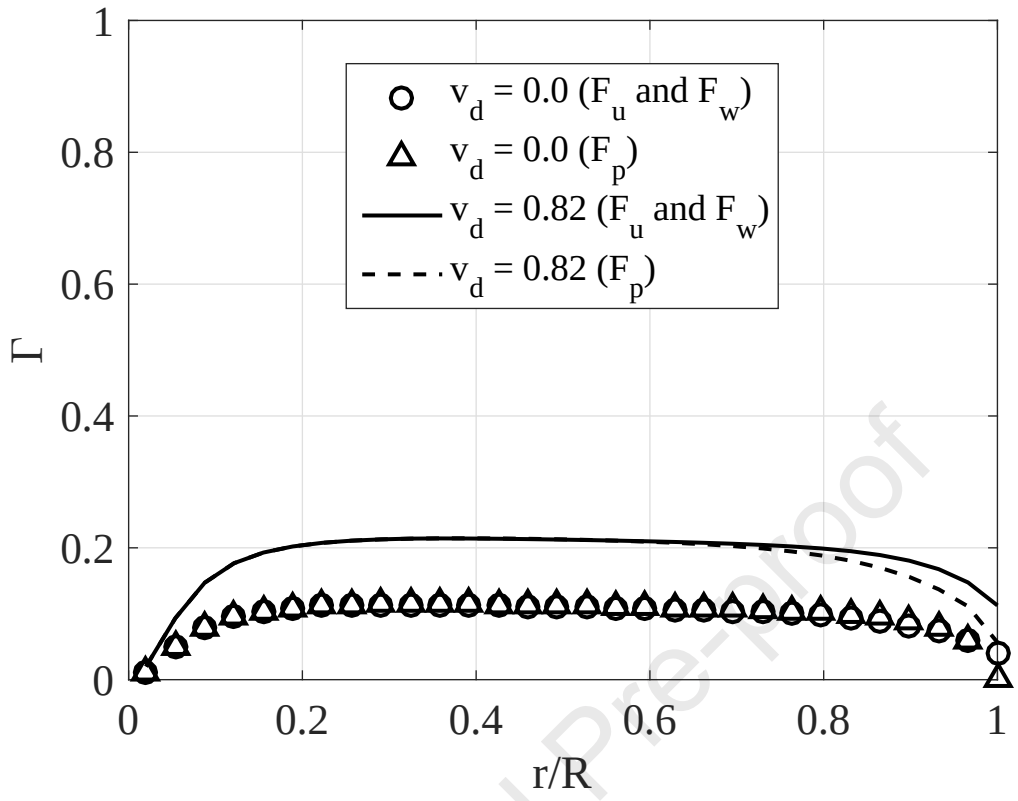

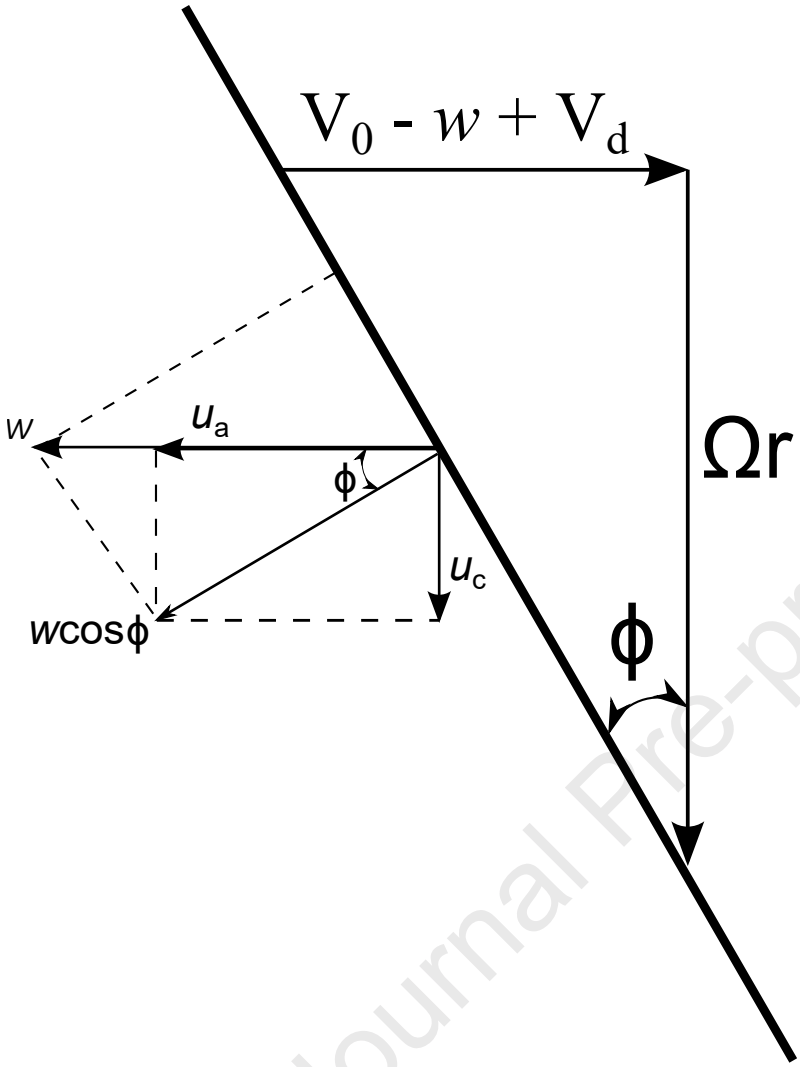

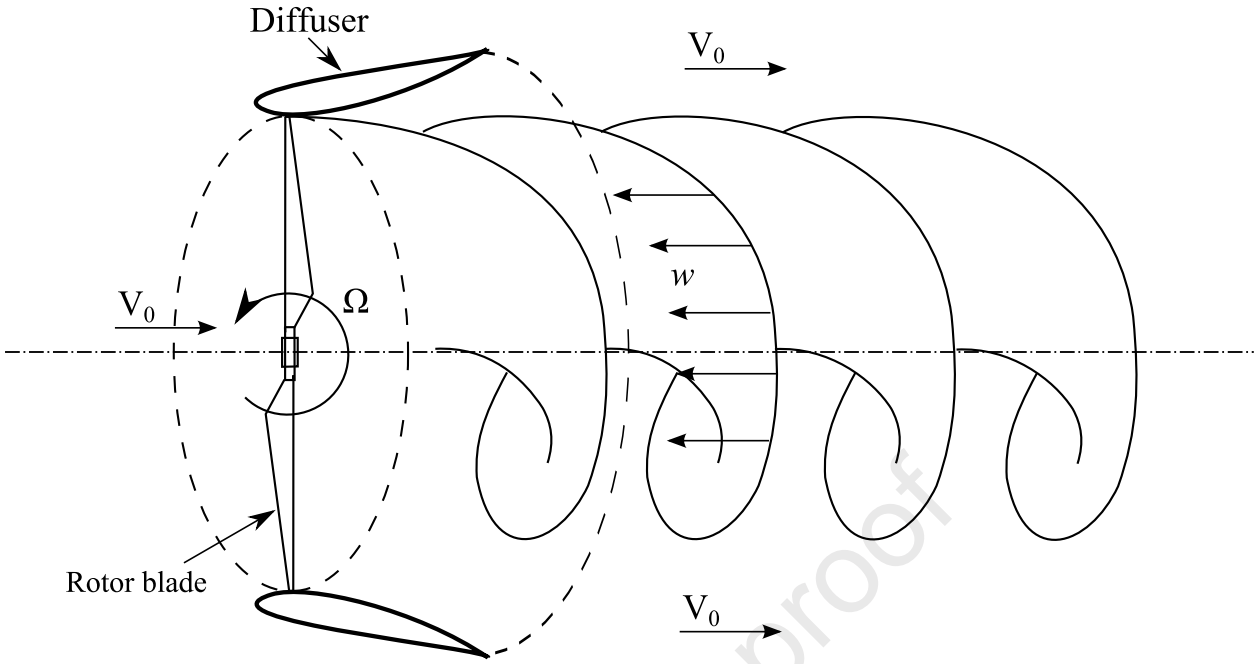

Highlights

- A new model for the finite number of blades in diffuser-augmented wind turbines;
- The blade loading is finite at the tip in contrast to bare turbines;
- Finite blade functions to optimize chord and twist angle of shrouded blades;
- Diffuser-augmented turbine power output seems to be less sensitive to tip speed ratio;
-Good agreement is demonstrated with available experiments.

Declaration of interests

☒ The authors declare that they have no known competing financial interests or personal relationships that could have appeared to influence the work reported in this paper.

☐The authors declare the following financial interests/personal relationships which may be considered as potential competing interests:

The authors declare no conflicts of interest.